ELECTRON ACCELERATION IN HELICON SOURCES

Francis F. Chen and Christopher D. Decker
University of California, Los Angeles, CA 90024-1594 USA

Abstract

Evidence is given for wave acceleration of primary electrons in a 1-cm radius helicon plasma source. The second root of the dispersion relation is also seen at low B fields. Electrostatic confinement of primaries appears to be important at these small diameters.

Plasma sources based on rf excitation of helicon waves have been shown to be unusually efficient (Boswell *et al.*, 1984, 1987). Chen (1985, 1989, 1991) has proposed that Landau damping causes efficient transfer of wave energy to the primary electrons. We give here experimental evidence for this hypothesis.

Helicon waves are bounded whistler waves in the frequency range well below the electron gyrofrequency but well above the lower hybrid frequency. Electron gyro-motions can then be neglected, together with all ion motions. The $E \times B$ motion of the electrons carries all the perpendicular current. In a bounded cylinder, the waves are not purely electromagnetic but have an important electrostatic component. For either an insulated or a conducting cylinder filled with uniform plasma of density n_0 in a uniform magnetic field B_0, waves of the form $\exp i(m\theta + kz - \omega t)$ follow the dispersion relation (Chen, 1989)

$$\frac{B_0}{n_0} = \frac{\omega}{k}\frac{\mu_0 e}{\alpha} , \tag{1}$$

where

$$\alpha^2 = T^2 + k^2 . \tag{2}$$

Here T is the transverse wavenumber determined by the boundary condition

$$m\alpha J_m(Ta) + kaJ_m'(Ta) = 0 , \tag{3}$$

which reduces to $J_1(Ta) = 0$ for the $m = 0$ mode, and $J_m'(Ta)$ is the r-derivative of the Bessel function $J_m(Tr)$ evaluated at $r = a$. With α from Eq. (2), Eq. (3) can be iterated to give T for each value of k. Eq. (1) then gives the value of B/n (in units of kG/10^{14} cm^{-3}) which is resonant with the wave (ω, k) for $m = 0$ and 1. Fig. 1 shows B/n plotted against $E_r = \frac{1}{2}m(\omega/k)^2$, an electron energy corresponding to the phase velocity, for a frequency of 31.2 MHz. Also shown is the computed damping length L_d due to both Landau and resistive damping.

Fig. 2 shows the apparatus. The quartz vacuum chamber is 1 cm in radius and 90 cm long. The magnetic field (0 – 1kG) can be swept from $B_{\max}$ to 0 in long (1 sec) pulses with a simple capacitor discharge circuit and is made uniform to ±5% to the end of the last coil by adjusting its current

separately. The discharge is grounded at the midplane port, which houses a Langmuir probe. At the ends, almost all the field lines flare out to end on the quartz wall rather than on the end flanges, unless intercepted by an endplate. Various types of probes and endplates are inserted from the end opposite the antenna. The rf amplifier, with a maximum output of 1 kW at 31.2 MHz, is coupled to the antenna through a low-loss, folded coaxial line with double-stub tuning. The reflected power is less than 1%. The antenna itself is a half-wavelength, $m = 1$ structure whose important elements are the two horizontal legs with oppositely phased currents. The following measurements were made under these fixed conditions: antenna length, 12 cm; frequency, 31.2 MHz; gas, Argon; pressure, 4 mTorr; rf power, 800W; termination, floating tantalum endplate covering the entire cross section.

The helicon resonance is shown in Fig. 3, where the density on axis, measured with the midplane probe, is plotted against magnetic field. The density is limited by the available rf power, which has to supply the radial losses (Chen, 1989). This maximum density, about 6×10^{12} cm^{-3}, is reached at about 100G. The linear part of the curve gives a constant value of B/n in agreement with Eq. (1), but the line does not go through the origin. There is apparently additional density due to non-resonant heating. At fields higher than 100G, the values of k excited by the antenna cannot satisfy Eq. (1), and the density falls in spite of the improving radial confinement. At very high fields, the discharge undergoes violent relaxation oscillations between resonant and non-resonant rf heating (Chen, 1989). At the lowest magnetic fields, the density rises again because of another resonance, which we believe to be the cyclotron root of the helicon dispersion relation.

Radial profiles of density and floating potential at the optimum field are shown in Fig. 4. For these dc measurements, rf fluctuations were filtered out with a choke located inside the probe shaft near the plasma.

From data such as shown in Fig. 3, we can compute the value of B/n, taking $\langle n \rangle \approx \frac{1}{2} n_{\max}$, according to the $n(r)$ shown in Fig. 4. For $\langle n \rangle = 3 \times 10^{12}$ cm^{-3} and $B = 100$ G, we obtain $B/n \approx 3.3$ (the data point shown in Fig. 1), corresponding to $E_r \approx 85$ eV. In other runs, B/n can differ by $\pm$ 25%. Furthermore, the collecting area of the probe tip cannot be measured to better than 10%. Because of the small slope of the B/n curve in Fig. 1, the value of E_r cannot be determined exactly. It can vary from 50 to 150 eV, a range in which the argon ionization cross section has a broad maximum.

Evidence of electron acceleration is seen in Fig. 5, showing the floating potential V_f of an endplate covering the entire diameter and located at the end of the uniform B-field region, 41 cm from the antenna. The endplate is charged negatively to < -200V when T_e is only a few eV, indicating the presence of fast electrons. The magnitude of V_f is consistent with a distribution of fast electrons with $\geq$ 50 eV energies. Moreover, since the density falls from the midplane to the endplate, B/n increases and k decreases (Eq. 1) as the waves propagate down the tube. Electrons trapped near the midplane can be accelerated to energies higher than 50 eV by the time they reach the endplate.

At $B = 20$ G, independent of the starting field $B_{\max}$, there is a jump in V_f to a less negative value. We believe that this is due to the scrape-off of those fast electrons which have acquired a large perpendicular velocity, since the Larmor radius of 50-eV electrons at 20G is equal to the tube radius. An idea of the acceleration length can be obtained by plotting the maximum $|V_f|$ vs. axial position (Fig. 6). The e-folding length is 15 cm, which lies in the range of damping lengths (1-50 cm) predicted by Fig. 1 for the measured range of B/n values. The fact that V_f rises for $B > 40$ G can be attributed to the cooling of the fast electrons with rising density. Above 100 G, the density no longer rises, but the helicon mode is no longer excited, again causing a decrease in the population of primaries and a rise in V_f. Such conjectural arguments may be too simplistic, however, because the axial variation of plasma light suggests a more complicated behavior, such as

the formation of double layers, which cannot yet be explored because of the sensitivity to insertion of axial probes, as indicated below.

Measurements with a small (8mm diam) end collector on axis showed the importance of discharge physics on helicon sources. The V_f of this collector was only a few volts negative, not 100-250V. We found two reasons for this. First, this collector intercepts field-aligned primaries from only a small tube of force near the axis, but this charge is canceled by ions attracted from the entire tube cross section. Second, the presence of the grounded tube supporting the probe greatly changed the nature of the discharge. With a large, floating endplate the plasma was dim near the end, since many of the fast electrons could not overcome the repelling potential of the endplate. With a grounded shaft, however, a large radial electric field develops, since the B-lines near the axis terminate at zero potential, while those on the outside terminate at large negative V_f. This radial E-field can trap primaries in large, axis-encircling orbits and allow them to go all the way to the end of the tube.

Though a complete understanding of the discharge physics is not yet in hand, we believe that we have shown helicon acceleration of electrons to energies near those at which the ionization cross section is near its maximum, thus explaining the efficient absorption of rf power in such discharges.

This work was supported by the National Science Foundation, Grant EC 89-02149.

References

Boswell, R.W. (1984) *Plasma Phys. and Controlled Fusion* **26**, 1147.

Boswell, R.W. and Porteus, R.K. (1987) *J. Appl. Phys.* **62**, 3123.

Chen, F.F. (1985) Australian National Univ. Report ANU-PRL IR 85/12 (unpublished).

Chen, F.F. (1987) in *Proceedings of the 1987 Int'l Conf. on Plasma Physics, Kiev, U.S.S.R.*, ed. by A.G. Sitenko (World Scientific, Singapore), Vol. 2, p. 797.

Chen, F.F. (1989) *Lasers and Particle Beams* **7**, 551.

Chen, F.F. (1991) *Plasma Phys. and Controlled Fusion* **33**, 339.

Figure Captions

1. Computed dispersion curves for $m = 0$ and 1 helicon waves at 31.2 MHz. Here B is in kG, n in units of 10^{14} cm^{-3}, and L_d (including collisions and Landau damping) in cm. E_r is the energy of an electron moving at the phase velocity. The dot is the experimental point for $n_{max} = 8 \times 10^{12}\,\mathrm{cm}^{-3}$ at $B = 100$ G.

2. Schematic of the apparatus.

3. Measured peak density vs. magnetic field.

4. Radial profiles of density (solid circles) and probe floating potential (open circles).

5. Floating potential of a large endplate vs. B-field.

6. Magnitude of the endplate floating potential vs. distance away from the antenna.

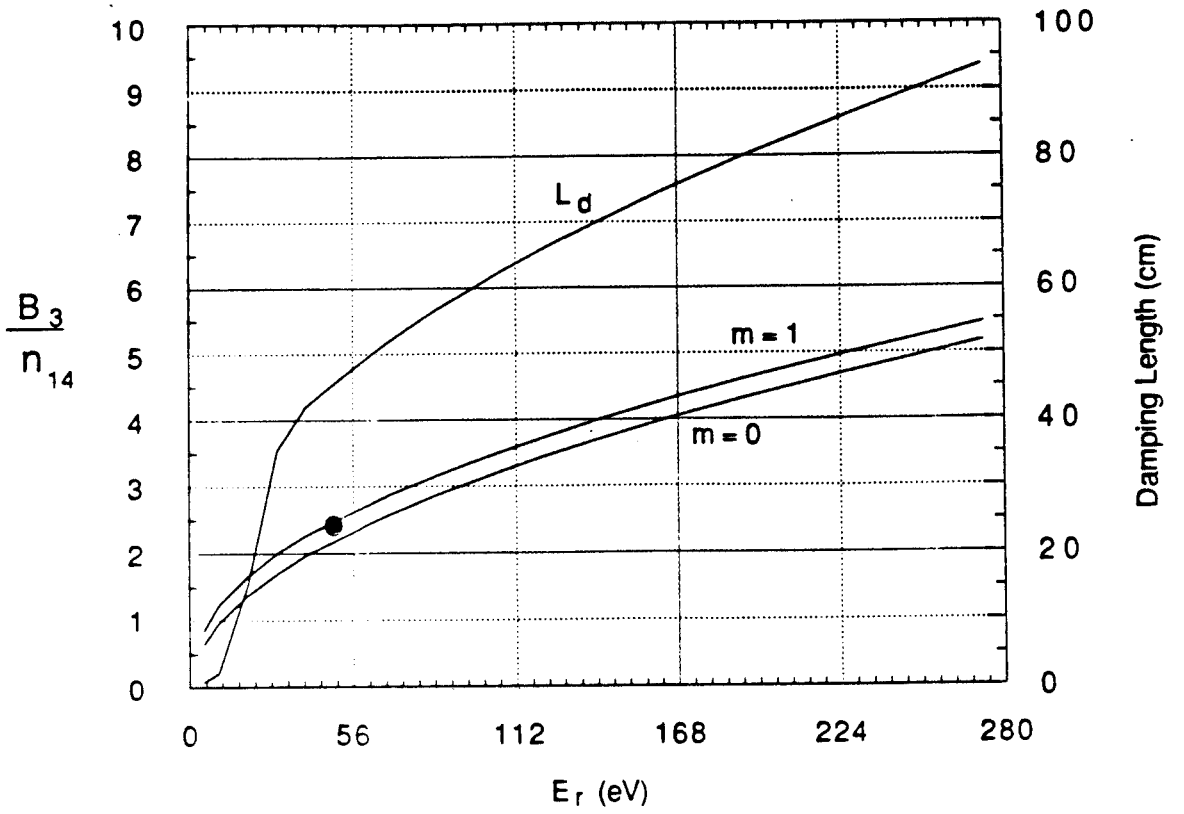

Figure 1

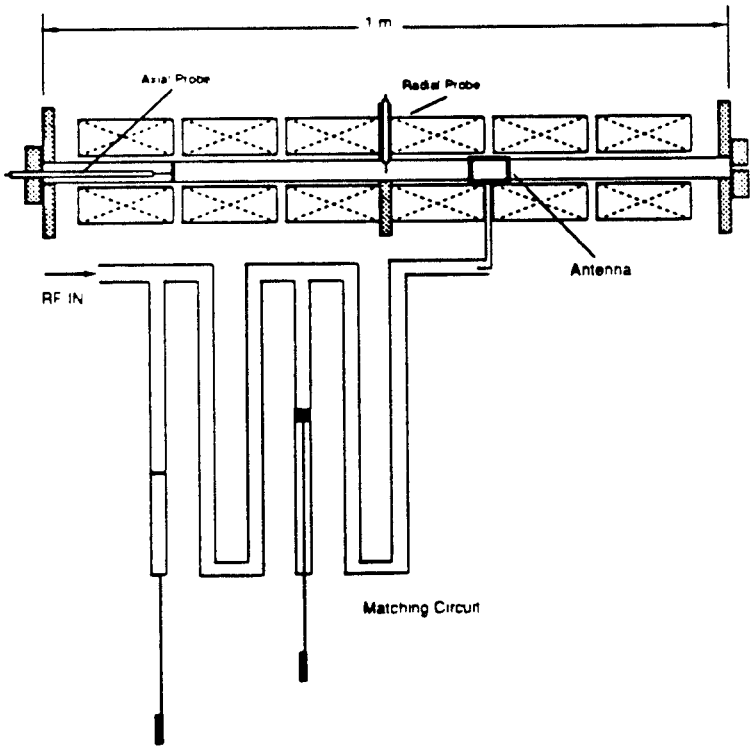

Figure 2

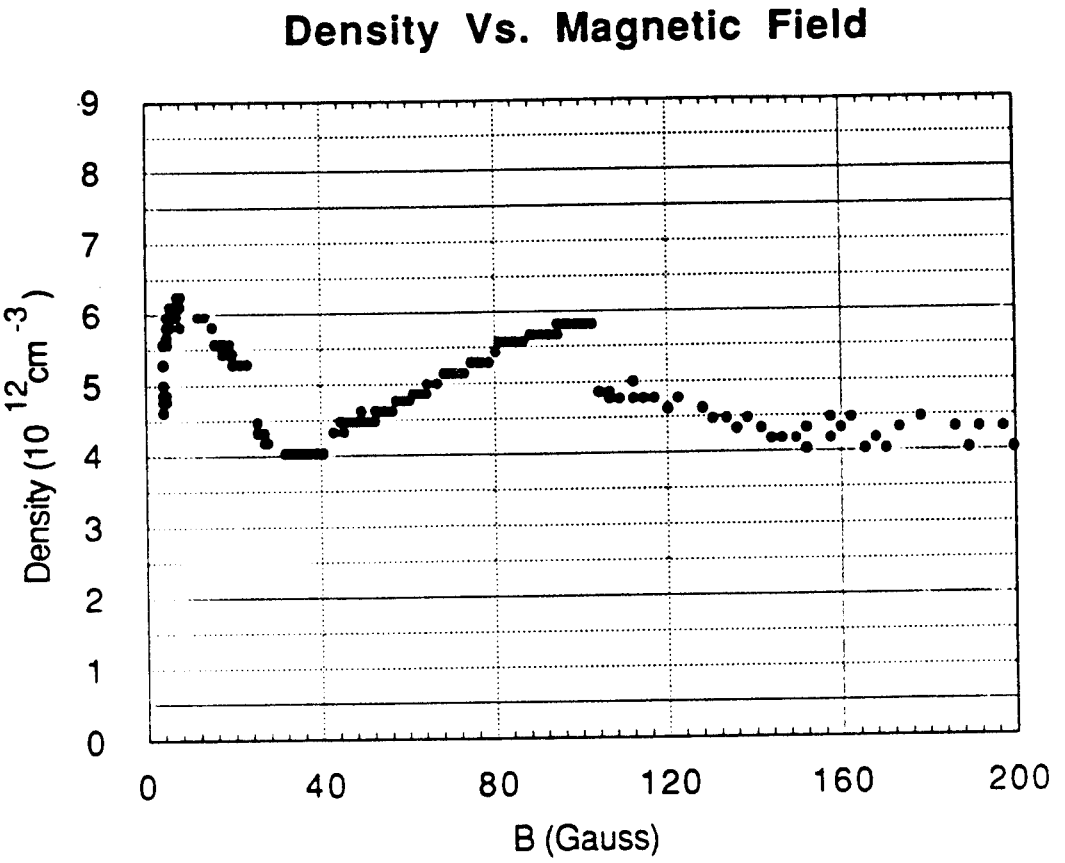

Figure 3

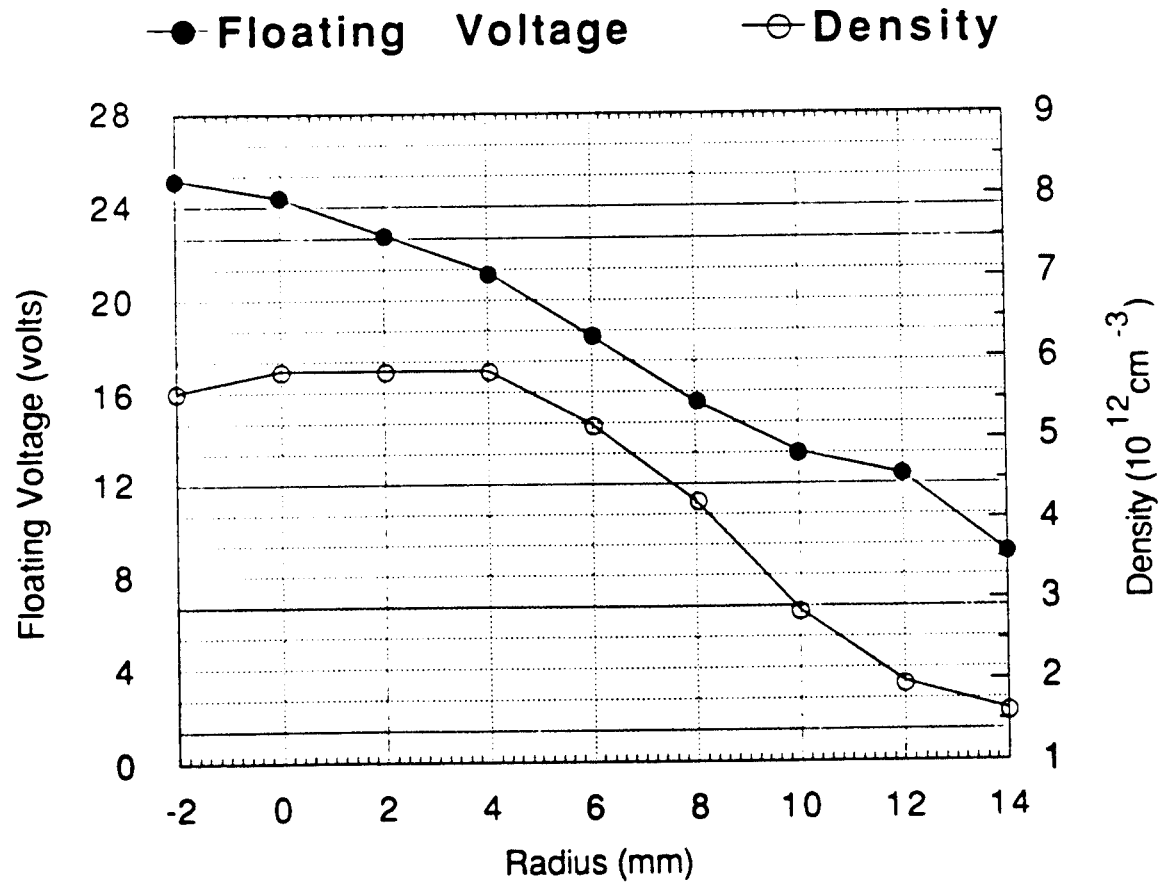

Figure 4

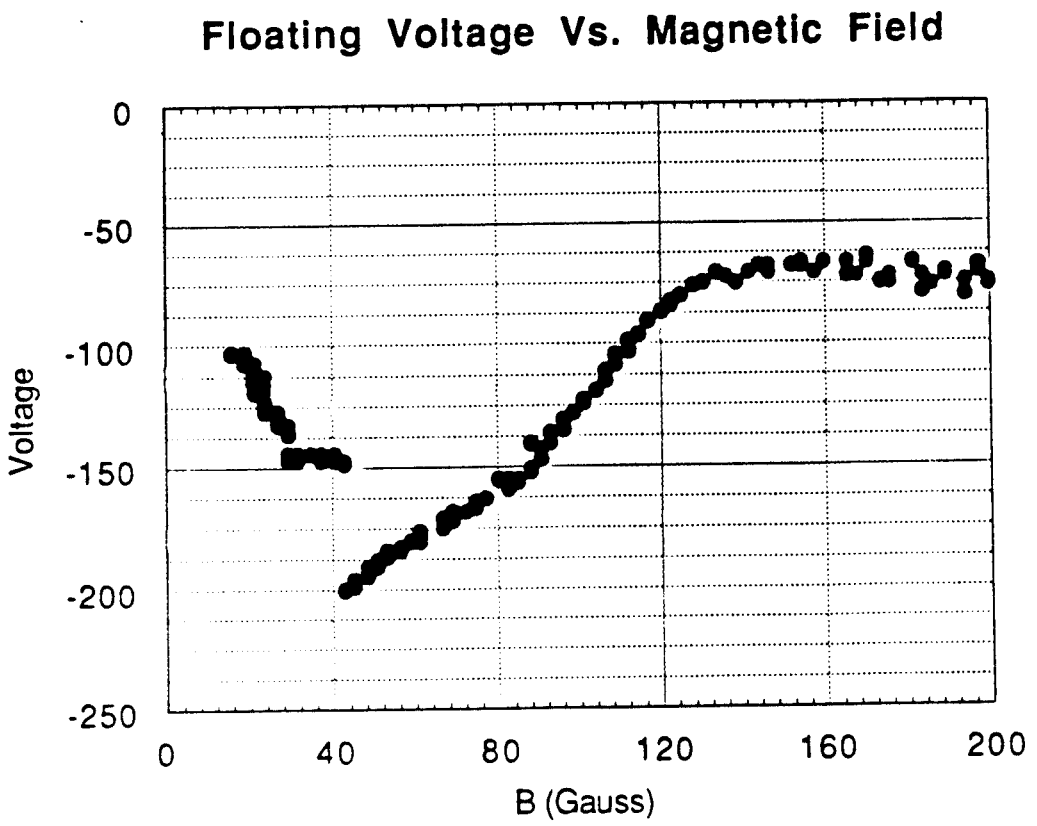

Figure 5

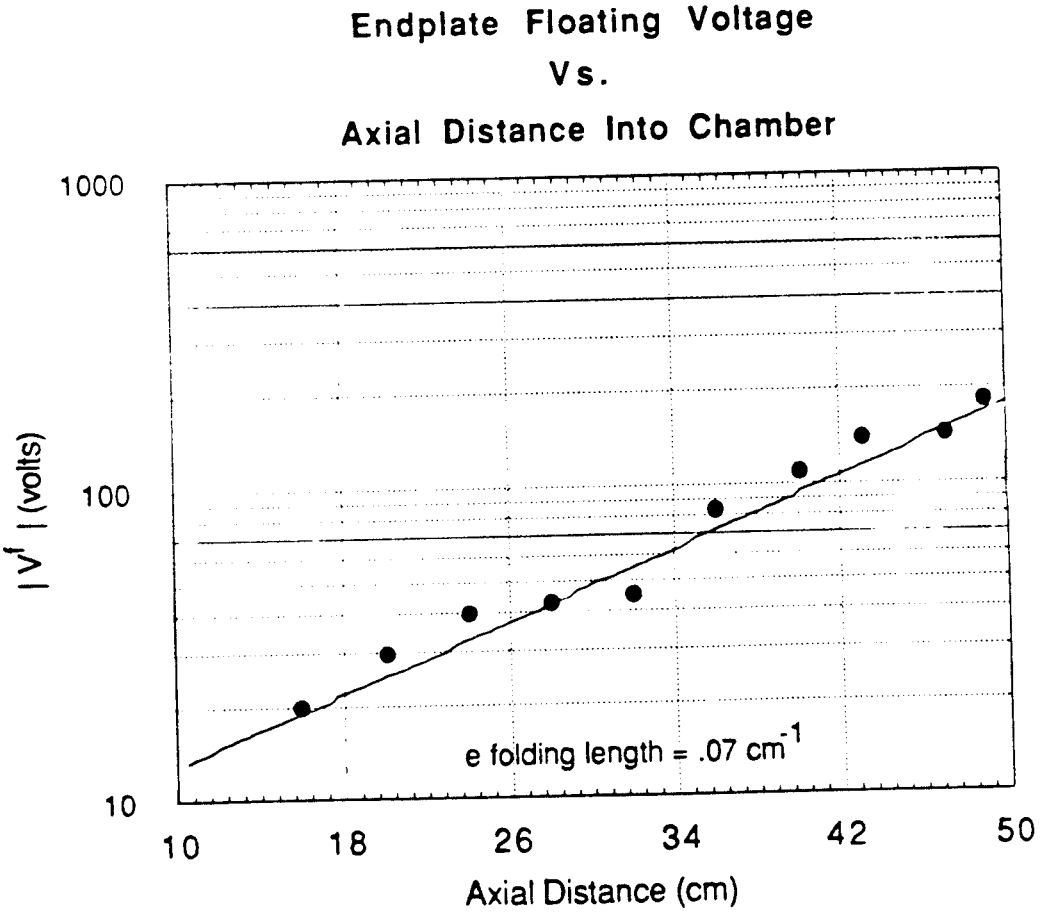

Figure 6